CONCRETE LIBRARY OF JSCE NO. 29, JUNE 1997

ANALYTICAL MODEL FOR FRACTURE BEHAVIOR OF PSEUDO STRAIN-HARDENING CEMENTITIOUS COMPOSITES

(Translation form Proceedings of JSCE, No.532/V-30, February 1996)

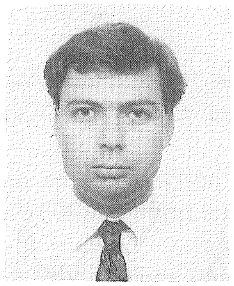

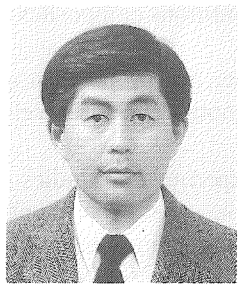

Petr KABELE

Hideyuki HORII

In the present paper we propose a simple analytical model for the fracture analysis of short-fiber reinforced cementitious composites designed to undergo distributed multiple cracking prior to formation of a localized crack under tensile and shear loading. The composite in the multiple cracking state is idealized as a homogenous and continuous material, with cracks being represented by cracking strain. A discrete crack model is used for localized cracks. The model is implemented in FEM code and experimental results are reproduced, proving the validity of the proposed model.

Keywords: *cementitious composites, short fibers, multiple cracking, localized cracking, analytical model, plasticity, discrete crack model*

Petr Kabele is an Assistant Professor in the Department of Civil Engineering at The University of Tokyo, Tokyo, Japan. He obtained his Ph.D. from The University of Tokyo in 1995. His research interests relate to material modeling and computational mechanics. He is a member of the JSCE.

Hideyuki Horii is a Professor in the Department of Civil Engineering at The University of Tokyo, Tokyo, Japan. He obtained his Ph.D. from Northwestern University in 1983. His research interests relate to applied mechanics, the mechanics of solids, rock mechanics, fracture mechanics, micromechanics, and the mechanics of materials. He is a member of the JSCE.

1. INTRODUCTION

In recent years, great attention has been paid to the development of high-performance structural materials for civil engineering applications. One group of such materials, called engineered cementitious composites (ECCs), has recently been developed by Li and co-workers [1], [2], [3]. Engineered cementitious composites are cement-based materials reinforced with short, randomly oriented and randomly distributed fibers. In contrast to other, usually quasi-brittle, short-fiber cementitious composites, the structure of ECCs is designed such that, under tensile and shear loading, they undergo multiple cracking accompanied by overall pseudo strain-hardening prior to the formation of a localized crack. Consequently, the fracture process zone in ECCs is not concentrated in a single plane or narrow band around the localized crack, but spreads over a large volume of the material. As a result of the extensive cracking away from the main crack plane, ECCs exhibit high fracture energy and critical tensile strain: up to two orders of magnitude higher than conventional cementitious composites with short fibers.

In the present paper, we propose an analytical model for the fracture analysis of structures made using ECCs. The motivation for developing such an analytical model for ECCs can be summarized as follows:

- Feedback to experimental studies: results of numerical analysis can be used to estimate the optimal setup for actual experiments, to verify experimental results, or to reveal the existence of phenomena which require further experimental investigation.
- Numerical experiments: physical experiments which are too expensive or difficult to carry out can be replaced by numerical experiments (this concerns, for example, investigations of the size effect, which would involve large specimens).
- Structural analysis: the analytical model can be used to conduct pilot studies on the applicability and feasibility of using ECCs in structural members.

In order to be able to accomplish these tasks, the model must adequately represent the presence of both multiple and localized cracking in ECCs. Furthermore, the model must be suitable for implementation into an FEM code so that structures of general geometries can be analyzed.

The earlier theoretical studies related to ECCs, e.g., by Li [4] and Li and Leung [5], mostly focus on the mechanics of a single crack with fiber bridging. These studies clarify the conditions for the development of multiple cracking. They also provide the link between composite micromechanical parameters (such as, fiber aspect ratio, fiber and matrix elastic moduli, matrix fracture toughness, fiber-matrix interfacial bond strength, etc.) and the bridging-stress to crack-opening-displacement (COD) relationship. Nevertheless, none of these studies provides an analytical model that could be directly implemented in an FEM code. Other well-established fracture models for cementitious materials, such as the fictitious crack model (FCM) proposed by Hillerborg et al. [6], do not consider the presence of an off-main-crack-plane multiple cracking zone and cannot be used alone for the analysis of ECCs.

In the present study, we idealize the composite undergoing multiple cracking as a homogenous and continuous material, with cracks being represented by additional (cracking) strain. With the help of the incremental theory of plasticity, we derive an incremental constitutive law for the composite in the multiple cracking state, and this is then directly used in an FEM program.

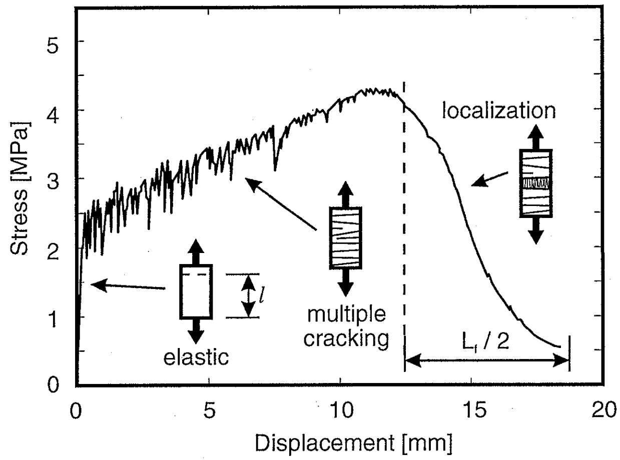

Fig. 1 Experimental [8] uniaxial stress-displacement curve for ECC with 2% by volume of polyethylene fibers

Localized cracks with bridging are modeled as discrete discontinuities in the displacement field. The discrete crack model is implemented into the FEM program with help of a cracked element developed by Nanakorn and Horii [7].

2. FRACTURE BEHAVIOR OF ECCS UNDER TENSILE AND SHEAR LOADING

The mechanism of tensile cracking in ECCs can be clarified by analyzing the results of uniaxial tension tests conducted by Li [1] and Maalej et al. [8]. **Figure 1** shows a typical uniaxial stress-displacement curve for an ECC specimen. The ECC in this case consisted of cement paste reinforced with 2% by volume of Spectra polyethylene fibers. The fiber length and diameter were 12.7 mm and 38 μm, respectively. The experiments revealed that, after formation of the first crack at a load magnitude equal to the first crack strength of the composite σ_{fc} , the material continued to sustain increasing loading. The increase in load was accompanied by the formation of additional subparallel cracks – a process called multiple cracking. Photographs taken during the experiment show that the cracks were more or less normal to the direction of the applied load. The pictures also suggest that during this process of multiple cracking, both crack openings and crack density increased with increasing load. As soon as the load reached a value hereafter referred to as the maximum bridging stress σ_{mb}, the specimen started to exhibit overall softening behavior. This transition into softening was associated with localization of the fracture into a single crack – apparently the one that had previously registered the largest COD. In the other words, after the peak, only one of the existing cracks continued to open while the others underwent unloading. The magnitude of the load during the post-peak part of the uniaxial test was controlled by the bridging stress transmitted across the localized crack. This stress decreased gradually with increasing COD of the localized crack, following a tension softening relationship.

Li [4] has shown that, if a random fiber distribution is assumed, the bridging stress should diminish when the value of COD reaches one half of the fiber length. It is seen from **Fig. 1** that if we subtract this value (in this case $L_f/2$ =6.35 mm) from the total displacement of the specimen when the stress just reaches zero, we obtain the approximate displacement at peak load. This means that the portion of total displacement associated with multiple cracking is not recoverable when the specimen is unloaded to zero stress.

It must be noted that, even though the total deformation of the specimen due to multiple cracking is relatively large, the high density of multiple cracks (several cracks per centimeter) ensures that their widths are very small, usually around 0.1 mm.

As Li and Leung [5] explain, multiple cracking results from properly designed fiber reinforcement; it occurs if, after a crack is formed, the bridging fibers undergo frictional debonding while transmitting increasing stress across the crack plane. The transition to softening mode is attributed to complete debonding of the bridging fibers and their slippage from the matrix.

Li et al. [9] also experimentally examined the structural response of shear beams made with ECCs. The specimens were reinforced by steel bars along the top and bottom surfaces in order to avoid flexural failure, but no conventional shear reinforcement was used. The ECC beams exhibited high ductility due to diagonal multiple cracking, which took place over a large volume of the material. The experiments confirmed that the behavior of ECCs under biaxial tension-compression stress is governed by the same phenomena that control the uniaxial behavior; that is, multiple cracking in a direction normal to the maximum principal stress and consequent localization into the crack with the largest COD. The experimental results also hinted that the compressive stress acting parallel to the cracks might positively influence the material strength. However, the experimental evidence so far is not sufficient to establish any relationship between the stress parallel to the crack direction and the first crack strength, the stress transfer capabilities of the bridging fibers, or the ultimate strength of the bridging. For this reason we will neglect this effect throughout the present study.

3. ANALYTICAL MODEL FOR ECCS

Due to the randomness of fiber orientation and distribution, and the short fiber lengths, ECCs are macroscopically homogenous and isotropic. The mechanical behavior of ECCs is dominated by the cracking they undergo in the process of loading. Therefore we treat ECCs in the proposed model as homogenous materials with cracks. Due to the different nature of the two types of cracking that occur in ECCs, we use different modeling approaches for distributed multiple cracking and for localized cracking.

3.1 Multiple cracking

Multiple cracking is characterized by the formation of a large number of relatively uniformly distributed subparallel cracks. The crack density is high while the crack widths are relatively small. In such a situation, it would not be practical to treat each crack separately. Instead, we idealize the composite undergoing multiple cracking as a continuous material with additional strain, called cracking strain, to represent the crack openings and density.

As discussed in the previous section, deformation resulting from multiple cracking is not recoverable upon unloading, which means that the cracking strain is inelastic. Considering further that a material in a multiple cracking state exhibits pseudo strain-hardening behavior, the strain-hardening theory of plasticity appears to be a suitable tool for modeling the multiple cracking that takes place in ECCs. The task is then to find a proper yield function and hardening rule.

a) Yield function and hardening rule

It was mentioned earlier that multiple cracking is initiated on planes normal to the maximum principal stress when the stress magnitude reaches the first crack strength. Keeping in mind that, when using the associated flow rule, the yield function not only determines the conditions for initiation of plastic yielding (or in our case multiple cracking) but also the direction of the plastic (or cracking) strain increment, we define the yield surface in the 2-D stress state using the Rankine yield function:

$$F \equiv \frac{\sigma_{xx}^{*}+\sigma_{yy}^{*}}{2}+\sqrt{\left(\frac{\sigma_{xx}^{*}-\sigma_{yy}^{*}}{2}\right)^{2}+\left(\frac{\sigma_{xy}^{*}+\sigma_{yx}^{*}}{2}\right)^{2}}-\sigma_{fc}=0 \tag{1}$$

where σ_{fc} is the first crack strength and $\sigma_{xx}^{*}, \sigma_{yy}^{*}, \sigma_{xy}^{*}$, and σ_{yx}^{*} are defined by the kinematic hardening rule as follows:

$$\sigma_i^{*}=\sigma_i-\alpha_i \tag{2}$$

Hereafter, i is used to represent the suffixes *xx*, *yy*, *xy*, and *yx*. Thus σ_i is a vector consisting of the in-plane components of the stress tensor. The vector α_i is defined by:

$$d\alpha_i=h\,d\varepsilon_i^{c} \tag{3}$$

in which $d\varepsilon_i^{c}$ is the cracking strain increment vector and h is a function of the total cracking strain, which reflects material hardening behavior.

It is seen from Eq. (2) that before any multiple cracking occurs (i.e., $\alpha_i=0$), σ_i^{*} is equal to the vector of in-plane components of the stress tensor. Therefore the first two terms of the yield function (Eq. (1)) initially correspond to the magnitude of the maximum principal stress in the x-y plane. Equation (1) thus satisfies the condition that multiple cracking is initiated when the maximum principal stress is equal to the first crack strength. It should be noted that we use Eq. (1) for both plane stress and plane strain; in the latter case we assume that the out-of-plane stress component σ_{zz} induces no cracking on planes parallel to x-y.

The associated flow rule, which we employ in the present model, implies that the cracking strain increment is proportional to the normal vector of the yield surface in stress space:

$$d\varepsilon_i^{c}=d\lambda\frac{\partial F}{\partial\sigma_i} \tag{4}$$

where $d\lambda$ is a non-negative scalar factor of proportionality. The normal vector $\partial F/\partial\sigma_i$ can be evaluated when substituting Eq. (1) as follows:

$$
\begin{aligned}
\frac{\partial F}{\partial \sigma_{xx}} &= \frac{1}{2} + \frac{\sigma_{xx}^* - \sigma_{yy}^*}{4\sqrt{\left(\frac{\sigma_{xx}^* - \sigma_{yy}^*}{2}\right)^2 + \left(\frac{\sigma_{xy}^* + \sigma_{yx}^*}{2}\right)^2}} \\
\frac{\partial F}{\partial \sigma_{yy}} &= \frac{1}{2} - \frac{\sigma_{xx}^* - \sigma_{yy}^*}{4\sqrt{\left(\frac{\sigma_{xx}^* - \sigma_{yy}^*}{2}\right)^2 + \left(\frac{\sigma_{xy}^* + \sigma_{yx}^*}{2}\right)^2}} \\
\frac{\partial F}{\partial \sigma_{xy}} = \frac{\partial F}{\partial \sigma_{yx}} &= \frac{\sigma_{xy}^* + \sigma_{yx}^*}{4\sqrt{\left(\frac{\sigma_{xx}^* - \sigma_{yy}^*}{2}\right)^2 + \left(\frac{\sigma_{xy}^* + \sigma_{yx}^*}{2}\right)^2}}
\end{aligned}
\tag{5}
$$

It is easy to show that if Eqs. (4) and (5) hold, then the maximum and minimum principal values of the cracking strain increment are:

$$
\begin{aligned}
\left(d\varepsilon^c\right)_1 &= d\lambda \\
\left(d\varepsilon^c\right)_2 &= 0
\end{aligned}
\tag{6}
$$

respectively, with the angle of the principal cracking strain increment $\theta^{d\varepsilon}$ being defined by:

$$
\tan\left(2\theta^{d\varepsilon}\right) = \frac{\sigma_{xy}^* + \sigma_{yx}^*}{\sigma_{xx}^* - \sigma_{yy}^*} \tag{7}
$$

Figure 2 shows that the incremental cracking strain $\left(d\varepsilon^c\right)_1$ in fact represents the incremental normal crack opening displacements of a set of cracks oriented at perpendicular to the direction $\theta^{d\varepsilon}$. Note that, consistently with this interpretation, the zero value of $\left(d\varepsilon^c\right)_2$ ensures that the cracks do not contribute to the deformation in a direction normal to $\theta^{d\varepsilon}$.

As angle $\theta^{d\varepsilon}$ may change throughout loading, an infinite number of sets of multiple cracks, each oriented at a different angle, may occur at any point in the material. It should be understood that this is a certain simplification of real material behavior; in reality, a small change in the principal stress direction would cause sliding of the existing cracks. But if the change in principal stress direction exceeds a certain limit, the formation of a new set of cracks would occur. However, to implement such mechanisms into the analytical model would require more experimental knowledge on the sliding behavior of cracks than is currently available.

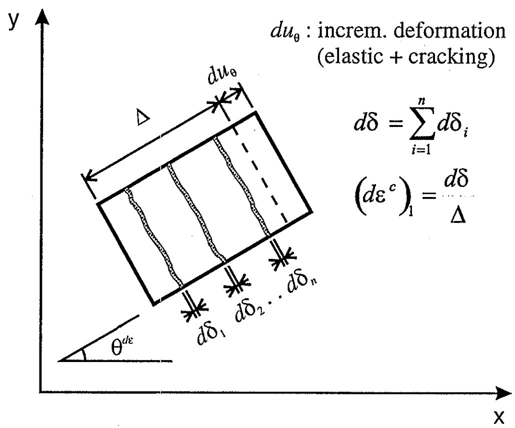

Fig. 2 Cracking strain increment to COD increment relationship

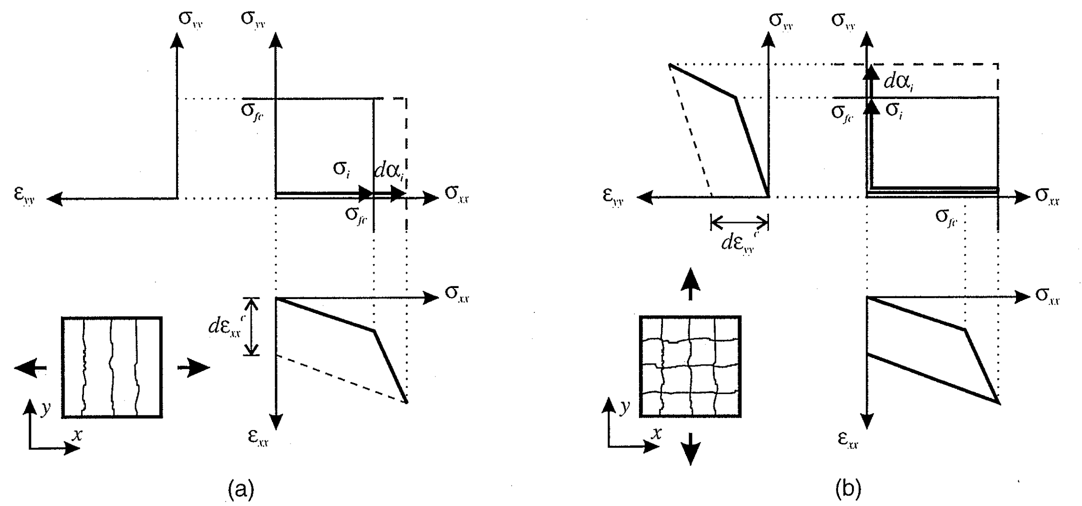

Fig. 3 Example of two-directional loading: (a) loading in x-direction; (b) unloading and reloading in y-direction

It was noted earlier that before multiple cracking occurs, σ_i^* is equal to σ_i. Thus, angle $\theta^{d\varepsilon}$ is initially equal to the angle of maximum principal stress θ^{σ}, which is defined by the following equation:

$$\tan\left(2\theta^{\sigma}\right) = \frac{\sigma_{xy} + \sigma_{yx}}{\sigma_{xx} - \sigma_{yy}} \tag{8}$$

The proposed model therefore correctly represents the experimental observation that the first set of multiple cracks is initiated on planes which are normal to the maximum principal stress.

The kinematic hardening rule defined by Eq. (2) implies that when the hardening takes place, the yield surface translates in the stress space in the direction of vector $d\alpha_i$ or, considering Eq. (3), in the direction of the cracking strain increment $d\varepsilon_i^c$. If the isotropic hardening rule were used, the yield surface would instead expand uniformly in stress space. To explain why we employ the kinematic hardening rule as opposed to the isotropic hardening rule, let us consider an example of two-directional loading as shown in **Fig. 3**. This figure shows the loading path and yield surface in the $\sigma_{xx} - \sigma_{yy}$ plane (top right), the stress-strain curves for x and y directions (bottom right and top left, respectively), and a schematic sketch of the cracked specimen (bottom left), at two different stages of loading: (a) and (b). Let us assume that the material is first uniaxially loaded in the direction of the x-axis – see **Fig. 3** (a). As the load reaches the first crack strength σ_{fc}, multiple cracking starts on planes normal to the x-axis, resulting in an incremental cracking strain whose only non-zero component is $d\varepsilon_{xx}^c$ as required by the associated flow rule and the shape of the yield surface. This is reflected in stress space by a translation of the original yield surface (which appears as two lines starting from point $[\sigma_{fc},\sigma_{fc}]$ and running parallel to the σ_{xx}- and σ_{yy}-axes) by an incremental vector $d\alpha_i$, which is parallel to the σ_{xx}-axis. It is seen in **Fig. 3** (b) that if the material is unloaded to zero stress and reloaded in the perpendicular direction (i.e., along the y-axis), the yield surface is reached when $\sigma_{yy} = \sigma_{fc}$. Further loading results in a cracking strain increment parallel to the σ_{yy} axis, i.e., the formation of a new set of cracks perpendicular to the existing ones.

If the isotropic hardening rule were used, initial loading in the x-direction would cause a uniform expansion of the yield surface. Then, upon reloading in the y-direction, no multiple cracking would take place until the yield surface is reached at a load level equal to the maximum load attained previously in the x-direction, which is higher than σ_{fc}.

As a result we can conclude that the present model based on the kinematic hardening rule reflects the assumption that, for a given direction, neither the first crack strength nor the hardening response of the cracked material are affected by the stress or cracking strain perpendicular to this direction.

Once the yield function and hardening rule are in place, the elasto-plastic incremental stress-strain relationship can be derived using the standard procedure adopted in the incremental theory of plasticity, as shown, for example, by Chen and Han [10]. It is noted that the elasto-plastic constitutive law is used only when the material undergoes plastic loading, i.e., when the following condition is satisfied:

$$\frac{\partial F}{\partial \sigma_i} d\sigma_i > 0 \tag{9}$$

where we apply the summation rule over index i = xx, yy, xy, and yx. If inequality (9) is not satisfied, the elastic stress-strain relation is used.
b) Treatment of the yield surface singularity
The only case which requires special attention while deriving the incremental elasto-plastic stress-strain relation is when:

$$\sigma^*_{xx} = \sigma^*_{yy} = \sigma_{fc} \text{ and } \sigma^*_{xy} = \sigma^*_{yx} = 0 \tag{10}$$

The equalities in Eq. (10) define the singular point of the yield surface. It is obvious that if we substitute Eq. (10) into Eqs. (5) we obtain the indefinite expressions 0/0, which means that the normal vector to the yield surface cannot be uniquely determined.

Various methods of handling yield surface singularities have been proposed in the literature [10], [11]. If the singularity is formed by the intersection of several smooth surfaces, then the plastic strain vector can be determined as a linear combination of the normal vectors of the adjacent surfaces. This approach, however, involves certain difficulties in the case of the Rankine yield function [11]. Another method is to replace the original yield function in a certain range around the singular point by another, smooth, function. Nevertheless, this approach requires introduction of an additional parameter (the size of the range to be replaced) and a smoothing function, and these are related rather to mathematical modeling than to the material's mechanical behavior.

In order to overcome these shortcomings we adopt yet another approach, which we now describe. The consistency condition requires that:

$$dF = \frac{\partial F}{\partial \sigma_i} d\sigma_i + \frac{\partial F}{\partial \alpha_i} d\alpha_i = 0 \tag{11}$$

It is obvious from Eq. (2) that:

$$\frac{\partial F}{\partial \alpha_i} = -\frac{\partial F}{\partial \sigma_i} \tag{12}$$

Then substituting Eq. (3) and Eq. (12) into Eq.(11) we get:

$$dF = \frac{\partial F}{\partial \sigma_i}\left(d\sigma_i - h\, d\varepsilon_i^c\right) = 0 \tag{13}$$

It can be shown that if the singular point defined by Eq. (10) is approached along the yield surface $F = 0$ from any given direction, then the normal vector $\partial F/\partial \sigma_i$ can be determined uniquely depending on this direction. In order to satisfy Eq. (13) at the singular point for any $\partial F/\partial \sigma_i$, i.e., if we approach the singular point from any direction, we must put:

$$\left(d\sigma_i - h\, d\varepsilon_i^c\right) = 0 \tag{14}$$

Then the following incremental stress-strain relationship can be obtained using Eq. (14), decomposing the strain increment into elastic and plastic (cracking) parts, and employing the elastic relationship between the stress increment and elastic strain increment.

$$d\sigma_i = \left(\frac{1}{h}\delta_{ij} + D_{ij}^e\right)^{-1} d\varepsilon_j \tag{15}$$

where δ_{ij} is the Kronecker delta operator and D_{ij}^e is the elastic compliance matrix.

It should be noted that Drucker's stability postulate implies that at the corner of the yield surface, the plastic strain vector must lie between the adjacent normals. This is also the condition for applicability of Eq. (15).

c) Material parameters

Equations (1) and (3) suggest that the model of multiple cracking is characterized by two material parameters – first crack strength σ_{fc} and a function h which reflects the shape of the hardening part of the stress-strain curve.

As shown in **Fig. 4**, both material parameters σ_{fc} and h can be easily determined from a uniaxial stress-strain curve. The hardening part of the stress-strain curve can be fairly well approximated by a linear relationship, which allows us to use a constant h.

3.2 Localized crack with bridging

In the model for multiple cracking described in the previous subsection, the cracking strain represents the density and width of the multiple cracks. The direction of the maximum principal cracking strain then can be interpreted as the direction normal to the most developed set of multiple cracks. Because the experimental results suggest that the focus of localization is in the one of the multiple cracks that has the largest opening displacement, we employ a condition for formation of the localized crack as follows: the localized crack is initiated on the plane normal to the maximum principal cracking strain when its magnitude reaches a certain critical value ε_{mb}^c. It has to be noted

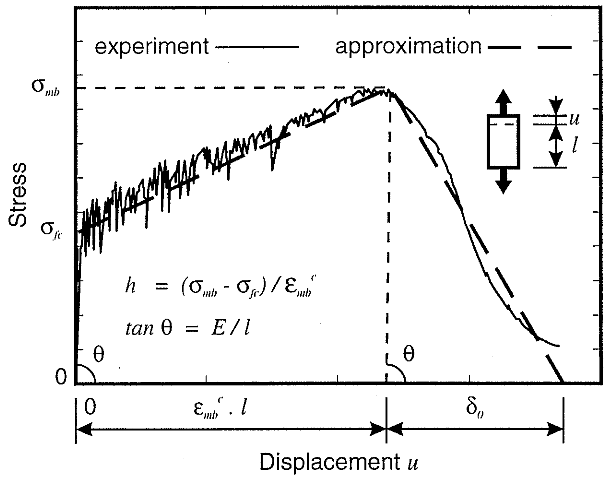

Fig. 4 Determination of material parameters from approximated uniaxial stress-displacement curve

that this condition is not sufficient to reproduce fracture localization in the case of a perfectly homogenous body with a uniform cracking strain field. In such a situation, the localization would have to decided by employing the thermodynamics-based theory for localization phenomena proposed by Horii and Okui [12].

Localized cracks are characterized by large opening displacements and by the existence of bridging. Therefore, the cracks are modeled as discrete discontinuities in the displacement field with the effect of bridging represented by traction applied to the crack surfaces.

Generally, both normal and tangential components of this traction are related to the relative displacements of the crack surfaces. However, for lack of experimental data on the shear behavior of localized cracks, we assume that once a localized crack is formed, normal bridging traction is related only to the normal COD, while the shear traction stays constant. The latter assumption is adopted only for simplicity and it will have to be modified if cracks undergoing relative shear displacement are to be correctly represented. The normal traction decreases with increasing normal COD according to the tension softening relationship, which is given in incremental form as follows:

$$dt_n = s\, d\delta_n \tag{16}$$

where dt_n stands for the increment in normal traction; s is the slope of the tension softening curve; and $d\delta_n$ is the incremental normal COD.

The expression given by Eq. (16) is valid only for cracks that are opening. There is no experimental information available on the response of localized cracks in ECCs during crack closure. Thus we use the widely accepted assumption that once a crack starts to close, normal traction decreases linearly with decreasing normal COD until it reaches zero at zero COD (neglecting the crack opening displacement gained during multiple cracking).

Note that, contrary to the model for multiple cracking, once a localized crack is formed at a certain point, its direction is fixed and no other localized crack opens in the same location. It is possible

Table 1 Material parameters for composites with various fiber volume fractions

V_f [%]	E [GPa]	n [-]	σ_{fc} [MPa]	ε^c_{mb} [%]	σ_{mb} [MPa]	δ_0 [mm]
0.8	10	0.2	2.0	2.27	2.85	6.27
1.0	10	0.2	2.0	2.82	3.05	6.17
2.0	22	0.2	2.2	5.78	4.32	6.62
3.0	10	0.2	2.5	6.15	4.97	5.28

however, that the material may undergo multiple cracking in the direction perpendicular to the localized crack.

Table 2 Dimensions of the DCB specimens

size	h [cm]	w [cm]	a_1 [cm]	a_2 [cm]
small	15.3	12.7	6.5	7.4
medium	30.0	31.0	11.7	14.7
large	58.5	49.0	13.4	21.5

The model for localized cracks is defined by two parameters: the critical cracking strain ε^c_{mb} and the tension softening curve. The value of ε^c_{mb} is determined from the results of the uniaxial tension test, as shown in **Fig. 4**. This figure suggests, that the post-peak part of the stress-displacement curve is almost linear, which allows us to make s constant. The value of s is then calculated as the negative ratio of normal traction transmitted across the crack when it is initiated at a critical cracking strain ε^c_{mb} to the critical crack width δ_o, which is determined from the uniaxial stress-displacement curve as shown in **Fig. 4**.

4. NUMERICAL RESULTS

The analytical model described in Section 3. has been implemented in an FEM program. The model for multiple cracking is implemented by means of an incremental constitutive law. For the localized crack model, we employ the cracked element developed by Nanakorn and Horii [7]. As all the governing equations are in incremental form, an algorithm based on the Euler method is used to integrate the incremental solutions.

In order to verify the performance of the proposed model we have used it to reproduce some experiments conducted on ECCs by Li and Hashida [3] and Maalej et al. [8]. These studies give experimental results for two types of test specimens: uniaxial tension (UT) specimens and double cantilever beam (DCB) specimens of various sizes. The material used in these experiments was a cement mortar reinforced with polyethylene fibers. The fiber volume fraction V_f is fixed at 2% in ref. [3] and varies between 0.2% and 4% in ref. [8].

4.1 Overall response and cracking behavior

Initially, we determined the material parameters from the experimental uniaxial stress-displacement curve of the composite with V_f equal to 2% (**Fig. 1**). These material parameters are listed in **Table 1**. Using these values, we analyzed the medium DCB specimen described in ref. [3]. The specimen geometry is shown in **Fig. 6** and its dimensions are listed in **Table 2**. The notch length used in this analysis was a_1=11.7 cm.

The specimen was discretized by a finite element mesh that initially consisted of 2,530 isoparametric quadrilateral 4-node elements. Some of these elements were, during the computation, automatically converted into cracked elements as a result of localized crack propagation. The mesh

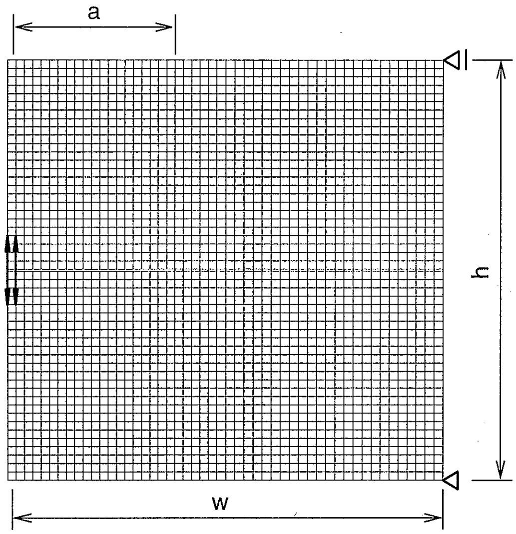

Fig. 5 Finite element discretization of the medium DCB specimen

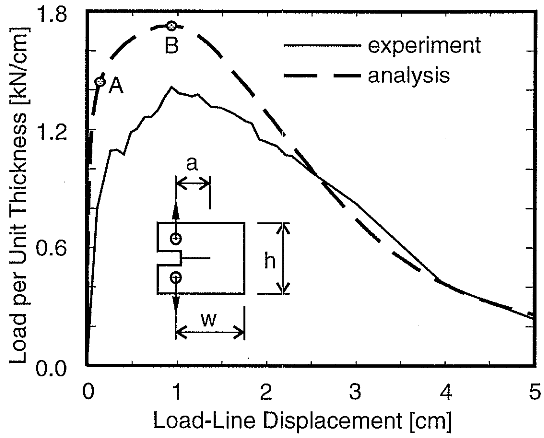

Fig. 6 Load-displacement curves for medium DCB specimen (V_f=2%)

is shown in **Fig. 5**. Note that due to material hardening behavior in the multiple cracking state and due to the transfer of bridging stress along the localized crack, the stress at the crack tip is bounded and the stress singularity vanishes. Thus, as far as overall behavior is concerned, the effect of the stress concentration at the crack tip is minor compared to the effect of the gradually expanding multiple cracking zone and the effect of fiber bridging across the localized crack. Accordingly, we employ an almost uniform mesh to reduce the influence of meshing on the development of the multiple cracking zone. Further, a sufficient number of elements in the ligament is necessary to ensure proper approximation of the COD along the localized crack once it propagates.

Figure 6 compares the experimental [3] and analytical load-displacement curves. This figure suggests that the proposed model is able to reproduce the presence of significant pre-peak nonlinearity, the displacement at the peak, and the post-peak branch of the load-displacement curve. The model, however, predicts a higher load at the peak. Possible reasons for this discrepancy will be discussed later.

Figure 7 shows the distribution of cracking strain and the evolution of the localized crack at different loading stages indicated by points A and B in **Fig. 6**. **Figure 7** (a) shows that before the bend-over point of the load-displacement curve, cracking is concentrated near the original notch tip. However, upon reaching the hardening portion of the curve, multiple cracking spreads rapidly around the notch tip while the evolution of the localized crack is relatively slow. In **Fig. 7** (b), the zone of multiple cracking has an onion-like shape at the peak load and it extends almost to the specimen boundaries; this is consistent with the experimental result. The direction of maximum principal cracking strain can be interpreted as normal to the most developed multiple cracks in **Fig. 7** (c), so the multiple cracking pattern and the extension of the localized crack are also in good agreement with the photographs of the cracked specimen provided in ref. [3].

4.2 Effect of fiber volume fraction

Maalej et al. [8] studied the influence of fiber volume fraction on the fracture energy of ECCs. They observed that the total fracture energy J_c of ECCs comprises of two components. The first, called the bridging fracture energy J_b, is associated with the fiber pull-out process on the main fracture plane. The second, denoted J_m, arises from distributed multiple cracking. A J-integral based technique was proposed for evaluating the total fracture energy J_c and component J_b. The total fracture energy was calculated using load-displacement curves for two DCB specimens differing only in original notch length. The bridging fracture energy was obtained from the post-peak portion of a uniaxial load-displacement curve. The fracture energy contributed by multiple cracking J_m is then obtained as the difference between J_c and J_b.

We attempted to reproduce the effect of fiber volume fraction on the composite fracture energy with the proposed model. The fiber volume fractions that we selected for our analysis were 0.8%, 1%, 2%, and 3%. As in the previous analysis, we first determined the material parameters for each volume fraction from its respective uniaxial stress-strain curve; the parameters are listed in **Table 1**. Then we computed the load-displacement curves for two DCB specimens with different initial notch lengths a_1 and a_2 for each volume fraction. To this end, we used the same specimen sizes as in the experimental study, i.e., a medium DCB with V_f equal to 0.8% and 1% and a large DCB with V_f equal to 2% and 3%. The exact dimensions of each specimen are listed in **Table 2**. Following the same procedure as in the experimental study [8], we calculated the fracture energies. The analytical results are compared with the experimental ones in **Fig. 8**. The figure shows that the proposed model reproduces the main feature: that with increasing fiber volume fraction, the fracture energy initially increases but later becomes saturated. The analytical results also confirm the experimentally elucidated feature that multiple cracking

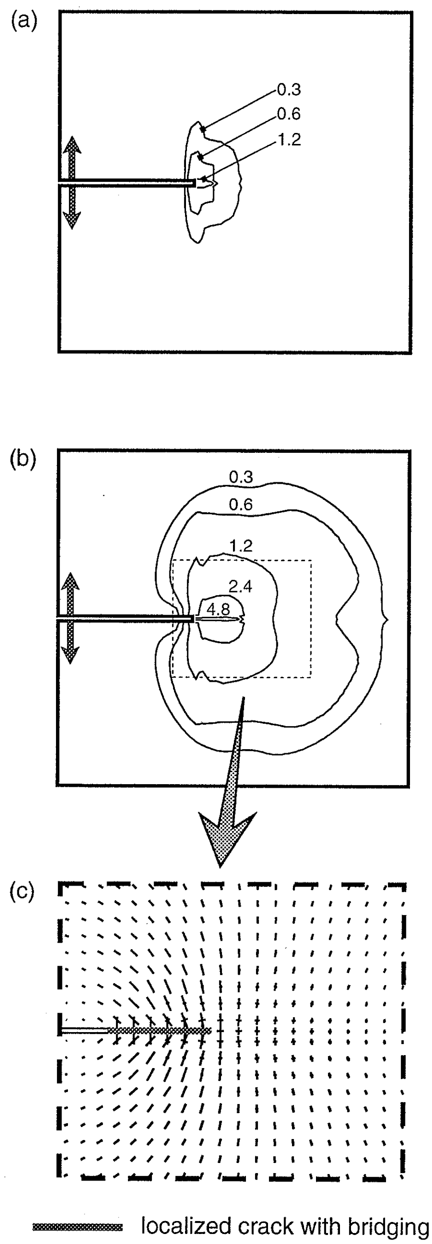

Fig. 7 Distribution of cracking strain and evolution of localized crack (medium DCB; a=11.7 cm; V_f=2%). (a), (b) contour lines of max. principal cracking strain [%] at load levels A and B, resp.; (c) principal cracking strain and localized crack in area near original notch tip at load level B

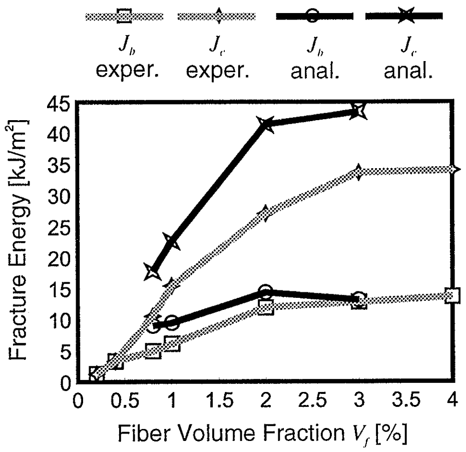

Fig. 8 Effect of fiber volume fraction on the total (J_c) and bridging (J_b) fracture energy

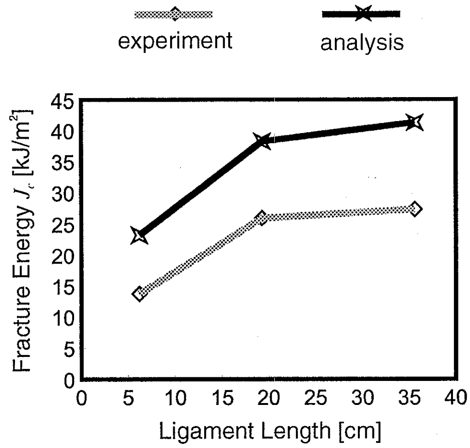

Fig. 9 Effect of specimen size on the total fracture energy J_c

contributes more than half of the total fracture energy for fiber volume fractions of 2% and 3%. The model, however, predicts higher magnitudes of total fracture energy, a result which can be attributed to overestimation of the peak load for the DCB specimens.

4.3 Effect of specimen size

Li and Hashida [3] and Maalej et al. [8] also observed that changing the specimen size while keeping the fiber volume fraction constant resulted in a change in the fracture energy. Namely, smaller specimens exhibited lower fracture energies. This phenomenon is explained by the fact that the size of a region that must undergo multiple cracking before steady state cracking is achieved is, in ECCs, up to several hundred square centimeters. If a specimen is very small, its boundaries limit the development of multiple cracking, which results in lower fracture energy.

In order to examine whether the proposed model can reproduce this feature, we computed the fracture energies for three different DCB specimen sizes: small, medium and large (see **Table 2**). The fiber volume fraction used in all of these analyses was 2%. **Figure 9** compares the analytical and experimental results. Total fracture energy J_c is plotted against initial ligament length (w-a_1), which was selected as representative of specimen size. It is clear that the proposed model correctly captures the fact that a small specimen gives a value of fracture energy almost fifty percent lower then the large one. Also consistent with the experimental result is the fracture energy for a medium beam, which is not much different from that of the large beam.

5. CONCLUDING REMARKS

The performance of the proposed analytical model for ECCs has been examined by analyzing the fracture behavior of DCB specimens. The results indicate that the model captures the characteristic behavior of ECCs fairly well, including the existence, extent, and orientation of multiple and localized cracking, trends of the load-displacement curve, and the effects of fiber volume fraction and specimen size on the fracture energy. The model, however, tends to overestimate the strength of DCB specimens and consequently the fracture energy. The reasons for this may be as follows.

- The number of experimental data used to obtain the material parameters, as well as in the comparison, was limited, so large errors may have been involved. (Only one pair of UT test data and DCB test data was available for most of the volume fractions examined.)
- The principal stresses in most of the region undergoing multiple cracking were tensile with minimum principal stress reaching the first crack strength. It is possible that the stress transfer capacity of bridging fibers is reduced by lateral tension. This possibility is currently being studied by analyzing other test specimens, such as shear beams.

The reasonable agreement between the analytical and experimental results confirms that the understanding of cracking behavior as outlined in Section 2. of this study is basically correct. However, more experimental work is needed to clarify the behavior of ECCs under biaxial loading, namely the effect of lateral stress on the hardening response of multiple cracks and on the composites' strength. If analysis of real structural members is to be carried out, more information about the response of localized cracks under relative shear displacement is also necessary.

Acknowledgment

The authors wish to express their sincere thanks to Professor Victor C. Li for his helpful discussions and for providing unpublished experimental data.

References

[1] Li, V.C., "From Micromechanics to Structural Engineering – The Design of Cementitious Composites for Civil Engineering Applications," Structural Eng./Earthquake Eng. Vol. 10, No. 2, pp.37-48, 1993

[2] Li, V.C., "Research Challenges in Toughness Development of Fiber Reinforced Cementitious Composites," Toughening Mechanisms in Quasi-Brittle Materials, S. P. Shah ed., Kluwer Academic Publishers, pp.447-466, 1991

[3] Li, V.C., and Hashida, T., "Ductile Fracture in Cementitious Materials?," Fracture Mechanics of Concrete, Z.P. Bažant ed., Elsevier Applied Science, London and New York, pp.526-535, 1992

[4] Li, V.C., "Postcrack Scaling Relations for Fiber Reinforced Cementitious Composites," J. of Materials in Civ. Eng., Vol. 4, No. 1, pp.41-57, 1992

[5] Li, V.C., and Leung, C.K.Y., "Steady State and Multiple Cracking of Short Random Fiber Composites," J. Eng. Mech., Vol. 118, No. 11, pp. 2246-2264, 1992

[6] Hillerborg, A., Modeer, M., and Peterson, P.E., "Analysis of Crack Formation and Crack Growth in Concrete by Means of Fracture Mechanics and Finite Elements," Cement and Concrete Research, Vol. 6, pp. 773-782, 1976

[7] Nanakorn, P., and Horii, H., "A Finite Element with Embedded Displacement Discontinuity," Building for the 21st Century, Y.C. Loo ed., Griffith University, Gold Coast Campus, pp. 33-38, 1995

[8] Maalej, M., Hashida, T., and Li, V.C., "Effect of Fiber Volume Fraction on the Off-Crack-Plane Fracture Energy in Strain Hardening Engineered Cementitious Composites," UMCEE Report No. 94-4, University of Michigan, Ann Arbor, Feb. 1994

[9] Li, V.C., Mishra, D.K., Naaman, A.E., Wight, J.K., LaFave, J.M., Wu, H.C., and Inada, Y., "On the Shear Behavior of Engineered Cementitious Composites," Advn. Cem. Bas. Mat., 1, pp. 142-149, 1994
[10] Chen, W.F., and Han, D.J., "Plasticity for Structural Engineers," Springer-Verlag, New York, 1988
[11] Pamin, J.K., "Gradient-Dependent Plasticity in Numerical Simulation of Localization Phenomena," Delft University Press, Delft, 1994
[12] Horii, H., and Okui Y., "Thermodynamics and Micromechanics-Based Continuum Theory for Localization Phenomena," Fracture of Brittle, Disordered Materials: Concrete, Rock and Ceramics, G. Baker and B.L. Karihaloo eds., E & FN Spon, London, pp. 391-405, 1995